

Gate-controlled valley transport and Goos-Hänchen effect in monolayer WS₂

Hassan Ghadiri¹ and Alireza Saffarzadeh^{2,3,*}

¹*Department of Physics, North Tehran Branch, Islamic Azad University, 16511-53311, Tehran, Iran*

²*Department of Physics, Payame Noor University, P.O. Box 19395-3697 Tehran, Iran*

³*Department of Physics, Simon Fraser University, Burnaby, British Columbia, Canada V5A 1S6*

(Dated: August 16, 2021)

Based on a Dirac-like Hamiltonian and coherent scattering formalism, we study spin-valley transport and Goos-Hänchen like (GHL) effect of transmitted and reflected electrons in a gated monolayer WS₂. Our results show that the lateral shift of spin-polarized electrons is strongly dependent on the width of the gated region and can be positive or negative in both Klein tunneling and classical motion regimes. The absolute values of the lateral displacements at resonance positions can be considerably enhanced when the incident angle of electrons is close to the critical angle. In contrast to the time reversal symmetry for the transmitted electrons, the GHL shift of the reflected beams is not invariant under simultaneous interchange of spins and valleys, indicating the lack of spin-valley symmetry induced by the tunable potential barrier on WS₂ monolayer. Our findings provide evidence for electrical control of valley filtering and valley beam splitting by tuning the incident angle of electrons in nanoelectronic devices based on monolayer transition metal dichalcogenides.

I. INTRODUCTION

Two-dimensional (2D) materials such as monolayers of transition metal dichalcogenides (TMDs) have attracted considerable attention due to their fascinating physical properties. In contrast to the zero-gap graphene, they are direct gap semiconductors with sizable bandgaps in the visible spectrum which make them promising materials in electronic and optoelectronic applications such as field-effect transistors and light-emitting diodes [1, 2]. The layered TMDs such as MoS₂ and WS₂ monolayers possess strong spin-orbit coupling due to the *d* orbitals of heavy metal atoms, causing a large spin splitting (~ 440 meV in WS₂ monolayers) in the valence bands [3, 4]. Moreover, the absence of inversion symmetry in the crystal structure of these materials allows valley polarization of carriers by optically exciting electrons with a circularly polarized light [5–10]. The valleys occur at the non-equivalent K and K' points in the hexagonal Brillouin zone of TMD monolayers [5]. Manipulating both the spin and valley degree of freedoms in such monolayers makes it possible to design new generation of nanoelectronic devices for quantum computing [5, 7, 8, 10].

It was demonstrated that the electrons and holes at the band edges of MoS₂ monolayers and other layered group-VI dichalcogenides can be well described by massive Dirac fermions with strong spin-valley coupling [5]. On the other hand, due to the similarities between propagation of Dirac fermions and propagation of electromagnetic waves in dielectrics, many optical phenomena such as Brewster angles [11], collimation [12], Bragg reflection, electronic lenses [13, 14] and Goos-Hänchen (GH) shift [15, 16] have been found in single-layer graphene. Among them, the GH effect refers to a lateral displacement of a light beam when it is totally reflected from a dielectric interface. In the past several years, most studies on the electronic GH shift have been devoted to graphene-based nanostructures such as graphene p-

n junctions [16], strained graphene [11, 17], graphene with electric and magnetic barriers [18, 19], and valley [17] and spin [20] beam splitters in graphene. Recently, the GH effect of electrons has also been studied in silicene [21] and a p-n-p junction of MoS₂ monolayer [22]. It was found that the GH shift of Dirac fermions, which has a magnitude of the order of Fermi wavelength [23, 24], can be amplified by multiple total internal reflections [22, 24]. Moreover, the lateral shifts of Dirac fermions in transmission through semiconductor barriers [25], graphene single barrier [23], double barrier [26], and multiple barrier structures [27] have also been reported. Such displacements, called Goos-Hänchen like (GHL) shifts, occur in the partial reflection regime and can be intensified by the transmission resonances (Fabry-Perot resonances). However, it is still a challenging problem to experimentally observe the GH or GHL shifts of electrons due to the smallness of the shifts and also the difficulty in producing a well-collimated electron beam [24]. On the other hand, to design a beam splitter effectively, the difference between lateral shifts of K and K' valley electrons should be greater than the width of incident electron beam which is about 100-1000 λ_F , with λ_F the Fermi wavelength of electrons [21, 26].

In this paper we study the quantum GHL effect of spin polarized electrons in transmission through a gated monolayer WS₂, acting as a tunable potential barrier, as shown in Fig. 1(a), in two cases of Klein tunneling and classical motion. We show that large positive and negative GHL shift values can be obtained in the transmitted and reflected electron beams. Moreover, the critical angle for total reflection of electrons at the interface between gated and ungated (normal) regions, is spin- and valley-dependent. Accordingly, it is possible to choose incident angles, so that spin-polarized electrons in one valley are allowed to propagate through the gated region, whereas the electrons in the other valley are blocked. We also show that the GHL effect can generate transmitted and reflected valley-polarized beams with a separation as large as the width of the incident beam, when a spin-polarized electron with a proper choice of energy is incident on the adjusted electrostatic barrier.

The paper is organized as follows. In section II, we intro-

*Electronic address: asaffarz@sfu.ca

duce our model and formalism for calculation of valley transport and GHM shifts for both transmitted and reflected electron beams. It is shown in section III for some limiting cases that our formalism can also reproduce the results of lateral shifts of *totally* reflected beam in MoS₂ [22] and graphene single interfaces [16], and also *partially* reflected electrons from graphene barrier [23]. Numerical results and discussions for spin-valley transport and lateral shifts in WS₂ monolayer, by tuning system parameters, are presented in Sec. IV. A brief conclusion is given in Sec. V.

II. MODEL AND FORMALISM

To explore the effect of GHM shift in a TMD monolayer with a tunable potential barrier, we consider a single-layer of WS₂ in $x - y$ plane and apply a top gate voltage to the region II ($0 < x < d$), while the regions I ($x < 0$) and III ($x > d$) are kept at zero electrostatic potential, as shown in Fig. 1. The top gate voltage induces a potential barrier with height V_G (Fig. 1(b)), and turn the system into a n-p-n WS₂ junction. This means that the electronic transport through the junction can be strongly affected by the gate. We emphasize here that the gate voltage in the proposed model is only utilized to shift the energy levels but not to modulate the energy gap. In this normal/gated/normal WS₂ junction, the low-energy electrons near valleys K and K' can be described by the Dirac-like Hamiltonian [5]

$$\mathcal{H} = at(\tau k_x \hat{\sigma}_x + k_y \hat{\sigma}_y) + \frac{\Delta}{2} \hat{\sigma}_z - \lambda \tau \frac{\hat{\sigma}_z - 1}{2} \hat{s}_z + V_G \Theta(x) \Theta(d - x), \quad (1)$$

where a is the lattice constant, t is the effective hopping integral, and $\tau = 1(-1)$ is the valley index corresponding to K (K') point. $k_{x,y}$ denote the components of electron wave vector measured from K and K', $\sigma_{x,y,z}$ are the Pauli matrices spanning the conduction and valence states in the two valleys, Δ is the band gap between valence and conduction bands, and 2λ is the spin-splitting at the valence band maximum due to the spin-orbit interaction. \hat{s}_z is the z component of Pauli matrix for electron spin and $\Theta(x)$ is the Heaviside step function. According to Eq. (1), the dispersion relation in the gated region II is given by

$$(2E - 2V_G - \tau s_z \lambda)^2 - (\Delta - \tau s_z \lambda)^2 = (2atk')^2, \quad (2)$$

where $k' = \sqrt{k_x'^2 + k_y'^2}$ and $s_z = \pm 1$ which stands for spin up (\uparrow) and spin down (\downarrow). In the regions I and III, however, the relation can be obtained by setting $V_G = 0$ and replacing k' with $k = \sqrt{k_x^2 + k_y^2}$.

Now we consider the propagation of spin-polarized electrons in the WS₂ junction which can be scattered by the potential barrier, induced by the gate voltage V_G . It is assumed that the spin-polarized electrons are injected by a magnetic contact, such as a ferromagnetic semiconductor [10, 28], into the left normal region. For simplicity, the source of spin injection is not included in the model. We further assume that the

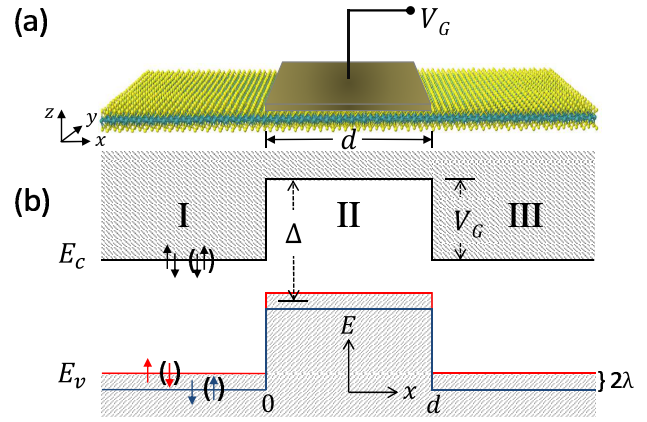


FIG. 1: (color online) Schematic model for the gated monolayer WS₂ in which the gated region acts as a tunable potential barrier. (b) Energy profile of the model shown in (a) for an incident electron with spin s_z (\bar{s}_z) in valley K (K') and a typical value $V_G < \Delta$. E_c and E_v denote the energy of conduction band minimum and valence band maximum, respectively. The red and blue lines show the spin-dependent energy levels at the top of the valence band, due to the spin-orbit coupling. Note that the spin splitting at different valleys are opposite due to the time-reversal symmetry.

dimension of monolayer along the y -axis is infinitely long. Therefore, due to the translational invariance in the y direction, k_y is conserved, and the electron wave function in each region can be described as

$$\psi_1 = \frac{1}{B_1} \begin{pmatrix} A_1 \\ \tau atk e^{i\tau\varphi} \end{pmatrix} e^{i(k_x x + k_y y)} + \frac{r_{s_z}^\tau}{B_1} \begin{pmatrix} A_1 \\ -\tau atk e^{-i\tau\varphi} \end{pmatrix} e^{i(-k_x x + k_y y)}, \quad (3)$$

$$\psi_2 = \frac{\alpha}{B_2} \begin{pmatrix} A_2 \\ \tau atk' e^{i\tau\varphi'} \end{pmatrix} e^{i(k'_x x + k_y y)} + \frac{\beta}{B_2} \begin{pmatrix} A_2 \\ -\tau atk' e^{-i\tau\varphi'} \end{pmatrix} e^{i(-k'_x x + k_y y)}, \quad (4)$$

$$\psi_3 = \frac{t_{s_z}^\tau}{B_3} \begin{pmatrix} A_3 \\ \tau atk e^{i\tau\varphi} \end{pmatrix} e^{i(k_x x + k_y y)}, \quad (5)$$

where $\varphi = \tan^{-1}(k_y/k_x)$ is the incident angle of electrons on the barrier, $r_{s_z}^\tau$ is the reflection amplitude, $\varphi' = \tan^{-1}(k_y/k'_x)$ is the angle of refraction, and $t_{s_z}^\tau$ is the transmission amplitude of electrons. The coefficients A_i and B_i ($i = 1, 2, 3$) in Eq. (3-5) are expressed as $A_1 = A_3 = E - \tau s_z \lambda + \Delta/2$, $A_2 = A_1 - V_G$, $B_1 = B_3 = \sqrt{A_1^2 + (atk)^2}$, and $B_2 = \sqrt{A_2^2 + (atk')^2}$.

The total internal reflection of electrons occurs if the incident electron waves strike the potential barrier at a critical angle φ_c which is given by

$$\varphi_c = \arcsin \sqrt{\frac{(2E - 2V_G - \tau s_z \lambda)^2 - (\Delta - \tau s_z \lambda)^2}{(2E - \tau s_z \lambda)^2 - (\Delta - \tau s_z \lambda)^2}}. \quad (6)$$

When the angle of incidence φ is greater than the critical angle, the electron wave vector in the electrostatic barrier, $k'_x = \sqrt{k'^2 - k_y^2}$, becomes imaginary which indicates an evanescent wave in the gated region, and hence, the electron beam will experience a total reflection from the electrostatic barrier. In the case of $\varphi < \varphi_c$, however, the electron wave is partially reflected and partially transmitted. The coefficients $r_{s_z}^\tau$, α , β , and $t_{s_z}^\tau$ can be obtained by applying the continuity of the wave functions at the two interfaces, $x = 0$ and $x = d$ shown in Fig. 1. The transmission $t_{s_z}^\tau$ and reflection $r_{s_z}^\tau$ coefficients for electron waves are expressed as

$$t_{s_z}^\tau = \frac{2ss' \sqrt{\frac{F_1}{F_2}} \cos \varphi \cos \varphi' e^{-ik_x d}}{2ss' \sqrt{\frac{F_1}{F_2}} \cos \varphi \cos \varphi' \cos(k'_x d) - iD}, \quad (7)$$

$$r_{s_z}^\tau = \frac{[-2ss' \sqrt{\frac{F_1}{F_2}} e^{i\tau\varphi} \sin(\tau\varphi') + i(1 - \frac{F_1}{F_2} e^{2i\tau\varphi}) \sin(k'_x d)] \sin(k'_x d)}{2ss' \sqrt{\frac{F_1}{F_2}} \cos \varphi \cos \varphi' \cos(k'_x d) - iD}, \quad (8)$$

where $D = [(1 + \frac{F_1}{F_2}) - 2ss' \sqrt{\frac{F_1}{F_2}} \sin \varphi \sin \varphi'] \sin(k'_x d)$, $F_1 = A_2/A_1$, $F_2 = (E - V_G - \Delta/2)/(E - \Delta/2)$, $s = \text{sgn}(A_1)$, and $s' = \text{sgn}(A_2)$.

To study the GHL effect, we consider an incident electron in the form of a Gaussian wave packet of width Δ_{k_y} and energy E ,

$$\psi_{in}(x, y) = \int_{-\infty}^{+\infty} dk_y f(k_y - k_{y_0}) \frac{1}{B_1} \times \left(\begin{array}{c} A_1 \\ \tau atk e^{i\tau\varphi(k_y)} \end{array} \right) e^{i[k_x(k_y)x + k_y y]}, \quad (9)$$

where the Gaussian $f(k_y - k_{y_0}) = e^{-(k_y - k_{y_0})^2 / 2\Delta_{k_y}^2}$ shows the angular distribution of electron beam around the central incidence angle $\varphi_0 = \arcsin(k_{y_0}/k)$. Therefore, the transmitted electron beam can be given as

$$\psi_{tr}(x, y) = \int_{-\infty}^{+\infty} dk_y f(k_y - k_{y_0}) \frac{t_{s_z}^\tau(k_y)}{B_3} \times \left(\begin{array}{c} A_3 \\ \tau atk e^{i\tau\varphi(k_y)} \end{array} \right) e^{i[k_x(k_y)x + k_y y]}. \quad (10)$$

In the case of $\Delta_{k_y} \ll k$, we can expand $\varphi(k_y)$ and $k_x(k_y)$ to first order around k_{y_0} , substitute in Eqs. (9) and (10), and evaluate the integrals, to obtain the spatial form of the incident and transmitted electron beams. In this regard, the incident beam is given by

$$\psi_{in}(x, y) = \frac{\sqrt{2\pi}\Delta_{k_y}}{B_1} \left(\begin{array}{c} A_1 e^{-(y-\bar{y}_+^{in})^2 \Delta_{k_y}^2 / 2} \\ \tau atk e^{-(y-\bar{y}_-^{in})^2 \Delta_{k_y}^2 / 2} e^{i\tau\varphi(k_{y_0})} \end{array} \right) \times e^{i[k_x(k_{y_0})x + k_{y_0} y]}, \quad (11)$$

where $\bar{y}_+^{in} = -\dot{k}_x(k_{y_0})x$, and $\bar{y}_-^{in} = -\dot{k}_x(k_{y_0})x - \tau\dot{\varphi}(k_{y_0})$. Here, the dot indicates the derivative with respect to k_y .

Therefore, the two components of ψ_{in} represent two Gaussians of the same width, centered at the two different mean coordinates \bar{y}_+^{in} and \bar{y}_-^{in} along the y-axis.

Using a similar analysis, the transmitted electron beam can be expressed as

$$\psi_{tr}(x, y) = \frac{\sqrt{2\pi}\Delta_{k_y}}{B_3} e^{i[k_x(k_{y_0})x + k_{y_0} y]} |t_{s_z}^\tau(k_{y_0})| \times \left(\begin{array}{c} A_3 e^{-\frac{1}{2}(y-\bar{y}_+^{tr})^2 \Delta_{k_y}^2} \\ \tau atk e^{-\frac{1}{2}(y-\bar{y}_-^{tr})^2 \Delta_{k_y}^2} e^{i[\tau\varphi(k_{y_0}) + \Phi_{t_{s_z}^\tau}(k_{y_0})]} \end{array} \right) \quad (12)$$

where $\bar{y}_+^{tr} = -\dot{k}_x(k_{y_0})x - \dot{\Phi}_{t_{s_z}^\tau}(k_{y_0})$ and $\bar{y}_-^{tr} = -\dot{k}_x(k_{y_0})x - \dot{\Phi}_{t_{s_z}^\tau}(k_{y_0}) - \tau\dot{\varphi}(k_{y_0})$. Note that $\Phi_{t_{s_z}^\tau}$ in Eq. (12) and in the mean coordinates \bar{y}_\pm^{tr} , denotes the phase of transmission coefficient $t_{s_z}^\tau$. Accordingly, the GHL shifts of the upper and lower components of the transmitted electrons are given by

$$\begin{aligned} \sigma_\pm &= \bar{y}_\pm^{tr}|_{x=d} - \bar{y}_\pm^{in}|_{x=0} \\ &= -\dot{\Phi}_{t_{s_z}^\tau}(k_{y_0}) - \dot{k}_x(k_{y_0})d. \end{aligned} \quad (13)$$

Since the two components have equal shift values, the average GHL shift of the transmitted beam can be expressed as

$$\sigma_{tr, s_z}^\tau = -\dot{\Phi}_{t_{s_z}^\tau}(k_{y_0}) - \dot{k}_x(k_{y_0})d. \quad (14)$$

Applying similar considerations to the lateral shift of the reflected beam, we find that $\sigma_+ = -\dot{\Phi}_{r_{s_z}^\tau}(k_{y_0})$ and $\sigma_- = \sigma_+ + 2\tau\dot{\varphi}(k_{y_0})$. By considering the probability of upper and lower components of the beams, the average shift of reflected electrons will be

$$\begin{aligned} \sigma_{re, s_z}^\tau &= \frac{1}{B_1^2} [A_1^2 \sigma_+ + (atk)^2 \sigma_-] \\ &= -\dot{\Phi}_{r_{s_z}^\tau}(k_{y_0}) + \frac{2\tau a^2 t^2 k^2}{B_1^2} \dot{\varphi}(k_{y_0}). \end{aligned} \quad (15)$$

In the case of transmitted beam, we need to calculate $\Phi_{t_{s_z}^\tau}$ from Eq. (7), and substitute into Eq. (14). Thus, the lateral GHL shift of transmitted electrons through the tunable electrostatic potential can be obtained by

$$\sigma_{tr, s_z}^\tau = \frac{[(8 + 2\frac{k_0^2}{k_x^2} + 2\frac{k_0^2}{k_x'^2}) \frac{\sin(2k'_x d)}{2k'_x d} - 2\frac{k_0^2}{k_x'^2}] d \tan \varphi}{4 \cos^2(k'_x d) + \frac{k_0^4}{k_x^2 k_x'^2} \sin^2(k'_x d)}, \quad (16)$$

where $k_0^2 = -ss'\gamma k k' + 2k_y^2$ and $\gamma = \sqrt{F_2/F_1}(1 + F_1/F_2)$.

On the other hand, by computing $\Phi_{r_{s_z}^\tau}$ from Eq. (8) and substituting into Eq. (15), the GHL shift for the reflected wave can be written as

$$\sigma_{re, s_z}^\tau = \sigma_{tr, s_z}^\tau + \frac{2\tau}{k_x} \left[\frac{C_1 + C_2 - C_3}{B_1^2(1 + C_0)} \right], \quad (17)$$

where

$$\begin{aligned} C_0 &= \left[\frac{F_1}{F_2} + 4\frac{k_y^2}{k'^2} - 2\frac{(k_x^2 - k_y^2)}{k^2} \right] \frac{F_1}{F_2} \\ &\quad - 4ss' \frac{k_y^2}{k k'} \left(1 + \frac{F_1}{F_2} \right) \sqrt{\frac{F_1}{F_2}}, \end{aligned} \quad (18)$$

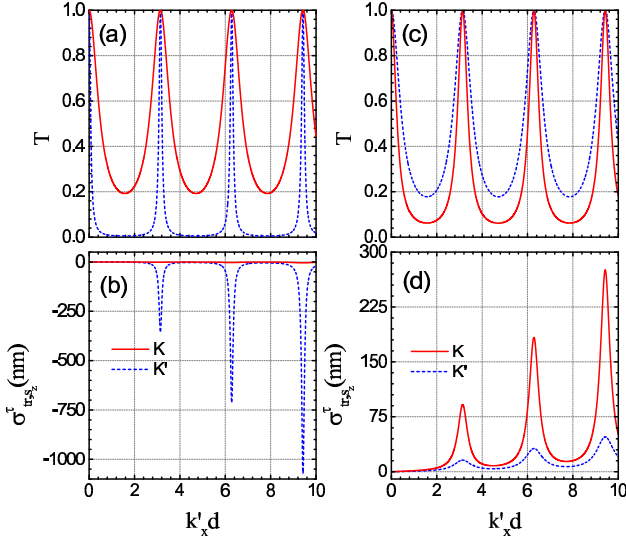


FIG. 2: (color online) Dependence of transmission probability and GH shift of the transmitted electrons with $s_z = 1$ on the width d of the gated region in (a,b) Klein tunneling and (c,d) classical motion, where $V_G = 3$ eV. The other parameters are: (a,b) $E = 1.75$ eV, $\varphi = 19.5^\circ$, and $\varphi_c = 50.10^\circ$ in K-valley, $\varphi_c = 20.51^\circ$ in K'-valley, (c,d) $E = 5.0$ eV, $\varphi = 20.5^\circ$, and $\varphi_c = 20.88^\circ$ in K-valley, $\varphi_c = 21.73^\circ$ in K'-valley. Note that d is normalized with k'_x .

$$C_1 = a^2 t^2 k^2 - A_1^2 \frac{F_1^2}{F_2^2} + (a^2 t^2 k^2 - A_1^2) \left[\frac{2k_y^2}{k'^2} + \frac{k_y^2 - k_x^2}{k^2} \right] \frac{F_1}{F_2}, \quad (19)$$

$$C_2 = ss' \left[k_x^2 (a^2 t^2 k^2 + A_1^2) - k_y^2 (a^2 t^2 k^2 - 3A_1^2) \right] \frac{1}{kk'} \sqrt{\frac{F_1^3}{F_2^3}}, \quad (20)$$

$$C_3 = ss' \left[k_x^2 (a^2 t^2 k^2 + A_1^2) + k_y^2 (3a^2 t^2 k^2 - A_1^2) \right] \frac{1}{kk'} \sqrt{\frac{F_1}{F_2}}. \quad (21)$$

It is important to note that the GH shift for the transmitted wave is dependent on the product of s_z and τ , as can be seen from the expressions, F_1 , F_2 , s , s' , and Eq. (2). In other words, the GH shift for the transmitted wave has a $s_z \cdot \tau$ (spin-valley) symmetry [29], whereas such a symmetry cannot be seen in the GH shift of the reflected wave, due to the presence of the second term in Eq. (17). In fact, the reflected beam is not only dependent on the product of τ and s_z , but also on valley index τ , separately, indicating that the reflected electron does not remain invariant under simultaneous interchange of spins and valleys in this system.

III. LIMITING CASES IN GH SHIFT

Now we consider some limiting cases to show how the present formalism is also able to reproduce the analytic results of previous studies in MoS₂ and graphene single interfaces [16, 22], and also graphene barrier [23].

A. single interface on TMD monolayers

As already mentioned, for incident angles greater than the critical angle, $\varphi > \varphi_c$, the wave vector k'_x becomes imaginary and hence, the total reflection occurs. In such a case, Eq. (17) which is given for $\varphi < \varphi_c$ is also valid for $\varphi > \varphi_c$, provided that we make the substitution $k'_x \rightarrow i\kappa$. After this substitution and taking the limit $d \rightarrow \infty$, the second term in Eq. (17) does not change, but the first term becomes

$$\frac{[8k_x^2 \kappa^2 + 2k_0^2 (\kappa^2 - k_x^2)] \tan \varphi}{\kappa (4k_x^2 \kappa^2 + k_0^4)}. \quad (22)$$

Therefore, the GH shift of the totally reflected beam from a step potential (single interface) applied on a monolayer of TMD, can be easily calculated by replacing the first term of Eq. (17) by (22).

In Ref. (22), the probabilities of upper and lower components of the reflected electrons have not been included in calculations and the average GH shift was simply computed by $\sigma_{re,s_z}^\tau = \frac{1}{2}(\sigma_+ + \sigma_-)$. On this basis, the second term in Eq. (17) becomes $\frac{\tau}{k_x} [1 - \frac{F_1^2}{F_2^2} - 2ss' \sqrt{\frac{F_1}{F_2}} (1 - \frac{F_1}{F_2}) \frac{k}{k'}] / (1 + C_0)$, and finally the GH shift of the totally reflected beam can be simplified as

$$\sigma_{re,total,s_z}^\tau = \frac{\frac{\tau}{k_x} [(\tau\kappa + k_y)^2 - k'^2 \frac{F_1}{F_2}] + \frac{2ss'k'}{\tau\kappa} (\kappa + \tau k_y) \sqrt{\frac{F_1}{F_2}} \cos \varphi}{(\tau\kappa + k_y)^2 + k'^2 \frac{F_1}{F_2} - 2ss'k'(\tau\kappa + k_y) \sqrt{\frac{F_1}{F_2}} \sin \varphi}. \quad (23)$$

This equation is exactly the same as Eq. (8) given in Ref. 22 for MoS₂ monolayers.

B. graphene barrier

By setting $\lambda = 0$ and $\Delta = 0$ in Eqs. (1), (16), and (17), the Hamiltonian of gapless graphene with a tunable potential barrier and the corresponding GH shifts for transmitted and reflected beams can be obtained, respectively [23]. In this regard, the lateral shifts of the reflected and transmitted electron beams in graphene are the same and expressed as

$$\sigma_{re} = \sigma_{tr} = \frac{[(2 + \frac{k_0^2}{k_x^2} + \frac{k_0^2}{k_y^2}) \frac{\sin(2k'_x d)}{2k'_x d} - \frac{k_0^2}{k_x^2}] d \tan \varphi}{\cos^2(k'_x d) + \frac{k_0^4}{k_x^2 k_y^2} \sin^2(k'_x d)}, \quad (24)$$

where $k_0^2 = -ss'kk' + k_y^2$. Note that in the case of $\lambda = 0$ and $\Delta \neq 0$ (gapped graphene), we obtain $\sigma_{re} \neq \sigma_{tr}$.

Eq. (24) at $ss' = \pm 1$ is the same as Eqs. (11) and (19) in Ref. 23, respectively. Moreover, in the case of $ss' = -1$, substituting $k'_x \rightarrow i\kappa$ for $\varphi > \varphi_c$ into Eq. (24), and taking the limit $d \rightarrow \infty$, one can obtain after some calculation

$$\sigma = \frac{k_y^2 - k k'}{\kappa k_x k_y}. \quad (25)$$

Finally, using Eq. (2), we obtain

$$\sigma = \frac{\sin^2 \varphi + 1 - V_G/E}{\kappa \sin \varphi \cos \varphi}. \quad (26)$$

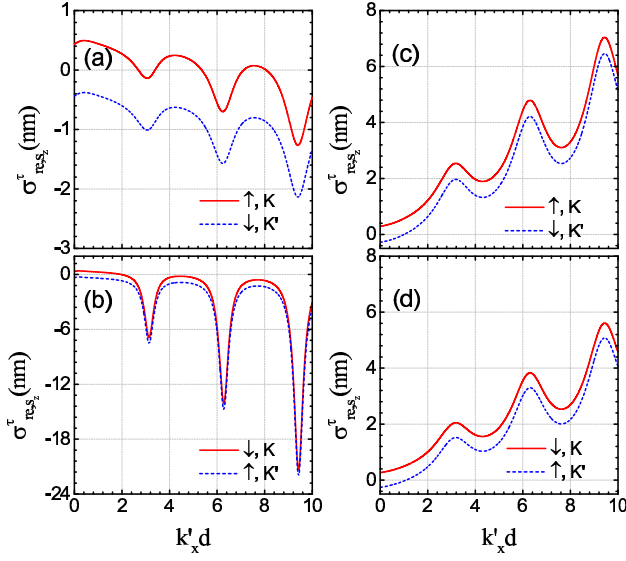


FIG. 3: (color online) Dependence of GH shift in the reflected beam on the width d of the gated region in (a,b) Klein tunneling and (c,d) classical motion, where for all plots $\varphi = 10^\circ$ and $V_G = 3$ eV. The other parameters are: (a) $E = 1.75$ eV and $\varphi_c = 50.10^\circ$, (b) $E = 1.75$ eV and $\varphi_c = 20.51^\circ$, (c) $E = 4.45$ eV and $\varphi_c = 14.75^\circ$, (d) $E = 4.45$ eV and $\varphi_c = 15.55^\circ$. Note that d is normalized with k'_x .

This equation describes the GH shift of electrons in total reflection from a step potential (single interface) on graphene. It is interesting to note that this expression is exactly the same as Eq. (11) given in Ref. 16. Therefore, our present formalism in limiting cases is able to reproduce the previous results of GH shifts for single interfaces on graphene [30] and TMD monolayers [22], and also GH shift on graphene barrier [23].

IV. RESULTS AND DISCUSSION

We present our numerical result for gated monolayer WS_2 as a family member of layered TMD materials, using the parameters $t=1.37$ eV, $\Delta=1.79$ eV, $2\lambda=0.43$ eV, and $a=3.197$ Å [5]. From the dispersion relation, Eq. (2), the energy regions for electrons in propagating mode are given by $\frac{\Delta}{2} < E < V_G - \frac{\Delta}{2} + \tau s_z \lambda$ and $E > V_G + \frac{\Delta}{2}$ associated with the Klein tunneling effect [23, 31–33] ($ss' = -1$) and the classical motion ($ss' = 1$), respectively. In both regimes, transmission probability, $T = |t_{s_z}^\tau|^2$, and lateral shift σ_{tr,s_z}^τ of electrons with energy value E and a given V_G , are strongly dependent on the width d of the gated region. Therefore, to compare these quantities in the two energy regions, we show in Fig. 2 the transmission probabilities and the GHL shifts of a transmitted electron beam with spin up ($s_z = 1$) through the gated monolayer, as the barrier width d (normalized by k'_x) is increased. At the resonance conditions $k'_x d = n\pi$ ($n = 0, \pm 1, \pm 2, \dots$), the potential barrier in both energy regions becomes fully transparent, $T = 1$, and the maximum absolute values of the lateral

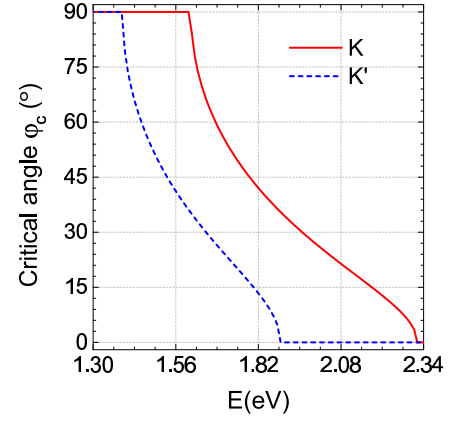


FIG. 4: (color online) Dependence of critical angles on incident energy for electrons with $s_z = 1$ in valleys K and K' at $V_G=3$ eV.

shifts are given by

$$\sigma_{tr,s_z}^\tau |_{k'_x d = n\pi} = \frac{k_0^2 d \tan \varphi}{2k_x'^2}. \quad (27)$$

Note that only the first three maxima are shown in Fig. 2(b) and (d). In the Klein tunneling regime (Fig. 2(a) and (b)), the transmission probabilities and the lateral shifts are strongly dependent on the valleys K and K', whereas such a valley-dependent transport is weaker in the classical motion as shown in Fig. 2(c) and (d). Although the angle of incidence is closer to the critical angles in the classical regime compared to the Klein tunneling regime, the GH effect in the Klein tunneling can more significantly separate the K and K' valley electron beams compared to the classical motion. For instance, the difference between the two lateral displacements at the third maximum absolute value is ~ 1065 nm in the Klein tunneling, while it is ~ 227 nm in the classical regime.

From Eq. (16), it is clear that the lateral shift is dependent on the angle of incidence. Moreover, k'_x is zero at critical angle φ_c . Therefore, at incident angles φ close to φ_c , the maximum absolute values of the shifts given by Eq. (27), can increase rapidly so that the spatial separation between K and K' electron waves in both regimes can exceed the width of incident beam. It should be mentioned that due to the presence of $s_z \cdot \tau$ symmetry in Eq. (16), the results given in Fig. 2 with $s_z = +1$ and $\tau = -1$ ($\tau = +1$) are the same as those with $s_z = -1$ and $\tau = +1$ ($\tau = -1$) (not shown).

We now study the effect of gated region on the reflected electron beam with some parameters different with those in Fig. 2. The GHL shifts as a function of normalized barrier width $k'_x d$ in the both regimes are shown in Fig. 3. In the Klein tunneling effect (Fig. 3(a) and (b)), the reflected K valley electrons exhibit positive or negative values of the lateral shifts, depending on the d values, whereas the GHL shifts of electrons belonging to the K' valley are only negative. In the classical motion regime (Figs. 3(c) and (d)), however, the reflected K' valley electrons can take positive or negative shift values, whereas the values are solely positive for the reflected beam belonging to the K-valley. The peaks

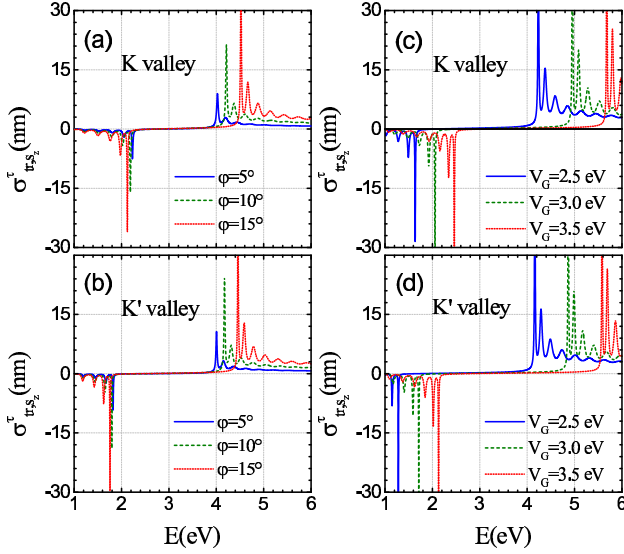


FIG. 5: (color online) The GHl shift of the transmitted K and K' electrons as a function of incident energy at (a,b) different incident angles and (c,d) different gate voltages. In (a,b) $V_G = 3.0$ eV, and (c,d) $\varphi = 20^\circ$. The width d of the gated region is fixed at 4 nm.

in σ_{re,s_z}^T correspond to the periodical occurrence of transmission resonances, as can be seen in the transmitted beam (see Fig. 2). Nevertheless, the lateral shift values at the resonance positions for the reflected electron beams are physically meaningless which is due to the fact that the reflection probability, $R = 1 - T$, at these positions is zero. In the vicinity of the resonances, the lateral shift of the reflected beam (similar to that of the transmitted beam) can increase rapidly when the incident angle approaches the critical angles.

As already mentioned, the $s_z \cdot \tau$ symmetry seen in the σ_{tr,s_z}^T does not exist in σ_{re,s_z}^T . Therefore, the values of lateral shifts for reflected K-valley electrons with spin s_z are different from those for K'-valley electrons with spin \bar{s}_z . As a result, the reflected electron beams from such electrostatic barriers are fully spin- and valley-polarized. However, as can be seen from Fig. 3, the lateral shift difference for the reflected electrons with the same value of $s_z \cdot \tau$ (in both regimes) is not enough to be detected experimentally, while it is detectable for electrons with different values of $s_z \cdot \tau$, when the incident angle is sufficiently close to φ_c (not shown).

From Eq. (6) it is clear that the critical angle φ_c for incident spin-polarized electrons with energy E is valley-dependent. Fig. 4 shows that how this angle for an incident electron with $s_z = +1$ and $\tau = \pm 1$ changes with energy. We can see that the values of φ_c within a specific energy window are quite different for the two valleys. This suggests that the incident angle φ can be tuned so that only electrons from a specific valley traverse through the electrostatic barrier, while the electrons from the other valley are fully reflected and blocked. For instance, for electrons with $s_z = +1$ and incident energy $E = 1.75$ eV, the critical angles in two valleys are $\varphi_c(\tau = 1) = 50^\circ$ and $\varphi_c(\tau = -1) = 20^\circ$ (see Fig. 4). Therefore, if the incident angle φ ranges between 20° and 50° , the K' valley electrons are backscattered, while the electrons be-

longing to the K-valley are transmitted, due to the different trajectories imposed by the gate voltage for each valley, indicating a valley filter with wide tunability.

The energy dependence of GHl shift for the transmitted K and K' valley electrons with $s_z = 1$ through the gated region with $d = 4$ nm is shown in Fig. 5. The lateral shifts of electrons at various angles of incidence (Figs. 5(a) and (b)) demonstrate successive peaks with different absolute values, corresponding to the transmission resonances, in both Klein tunneling and classical motion regimes with positive and negative lateral shifts, respectively. The almost zero lateral shift region between Klein tunneling and classical motion is the transmission gap [34] and is given by $V_G + \frac{1}{2}\tau s_z \lambda - \frac{1}{2}\sqrt{4a^2 t^2 k_y^2 + (\Delta - \tau s_z \lambda)^2} < E < V_G + \frac{1}{2}\tau s_z \lambda + \frac{1}{2}\sqrt{4a^2 t^2 k_y^2 + (\Delta - \tau s_z \lambda)^2}$, which includes the energy gap as well.

Clearly the transmission gap can be wider and the absolute values of the lateral shifts, as well as their difference belonging to different valleys, can be enhanced by increasing the angle of incidence. Moreover, by comparing the energies of maximum absolute values of GHl shifts for K and K' electrons, we can see that the valley separation in the case of Klein tunneling is stronger than that in the classical motion [10]. Figs. 5(c) and (d) illustrate the effect of various gate voltages on GHl shift of the transmitted K and K' electrons, when the incident angle is 20° . Here, one can see that the transmission gap also increases with increasing the external gate. In addition, with increasing the gate voltage, the whole spectrum of the lateral shifts moves towards higher energies and the maximum absolute values of the shifts as well as their differences, increase.

Note that due to the time reversal symmetry, the lateral shifts of incident electrons with spin $s_z = -1$, remain unchanged, if we interchange the valleys in the transmitted beam, while the lateral shifts will be somewhat different by interchanging the valleys in the reflected electron beams (not shown) due to the absence of $s_z \cdot \tau$ symmetry, as discussed previously.

In order to explore the influence of a continues range of gate voltages on the GHl shift, in Fig. 6 we show the calculated results for transmitted K and K' electrons with spin $s_z = 1$ and energy $E = 2.5$ eV, when the external gate is varied from 0.5 to 4.5 eV. The lateral shifts of both K and K' electrons are positive at low gate values, due to the classical motion of electrons which satisfy the condition $E > V_G + \frac{\Delta}{2}$ for any incident angle $\varphi < \varphi_c$. However, at higher gate voltages, the incident electrons experience the Klein tunneling effect, and hence, the lateral shifts become negative. Again, there is a gap-like feature in the lateral shift values between the classical motion and Klein tunneling regimes, corresponding to the transmission gap. As the incident angle increases, the maximum absolute values of the lateral shifts as well as their differences increase and the gap-like region becomes broader.

Comparing the gate voltages at which the absolute values of the lateral shifts in the two valleys are maximum, we can see that at some gate values the shift of K' valley electrons in the Klein tunneling is almost zero, while the shift of K

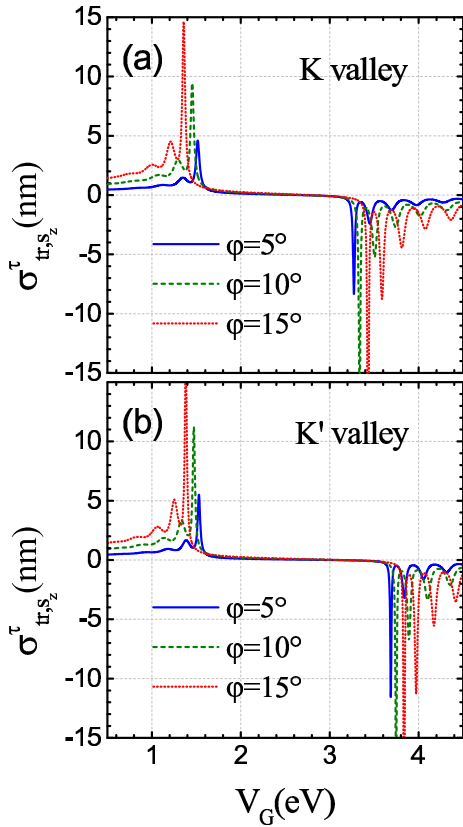


FIG. 6: (color online) Gate voltage dependence of GHL shift for transmitted K and K' electrons with $s_z = 1$ at three different incident angles. The incident energy E and the width d of the gated region are fixed at 2.5 eV and 4 nm, respectively.

valley electrons is maximum. As already mentioned, these maximum values correspond to the transmission resonances and demonstrate the valley splitting of charge carriers in WS₂ monolayers, which can be generated and controlled by gate voltage [8, 10].

V. CONCLUSION

In conclusion, the spin-valley transport and the GHL effect of the transmitted and reflected electrons in a WS₂ monolayer with a tunable electrostatic barrier have been theoretically studied in both Klein tunneling and classical motion regimes. Interestingly, it was found that the GHL shift of the reflected electrons does not remain invariant under simultaneous interchange of spins and valleys. Therefore, the spin-valley symmetry in the lateral shifts of the reflected electrons from the barrier is different compared to that in the transmitted electrons. The lateral displacement of electron beams can be positive or negative dependent on the width of the gated region and/or incident energy. Our findings show that a valley filter and valley beam splitter can be achieved by tuning the incident angle of electrons and external gate voltage in WS₂ monolayers. These features indicate the possibility of manipulating valley index in the TMD monolayers which can be utilized for quantum information applications [10].

Acknowledgement

This work is partially supported by Iran Science Elites Federation.

-
- [1] Q. H. Wang, K. Kalantar-Zadeh, A. Kis, J. N. Coleman, and M. S. Strano, *Nat. Nanotech.* **7**, 699 (2012).
- [2] S. Jo, N. Ubrig, H. Berger, A. B. Kuzmenko and A. F. Morpurgo, *Nano Lett.* **14**, 2019 (2014).
- [3] B. Zhu, X. Chen, and X. Cui, *Sci. Rep.* **5**, 9218 (2015); Z. Ye, T. Cao, K. Ó'Brien, H. Zhu, X. Yin, Y. Wang, S.G. Louie, and X. Zhang, *Nature* **513**, 214 (2014).
- [4] S. Salehi and A. Saffarzadeh, *Sur. Sci.* **651**, 215 (2016).
- [5] D. Xiao, G-B Liu, W. Feng, X. Xu and W. Yao, *Phys. Rev. Lett.* **108**, 196802 (2012).
- [6] W. Yao, D. Xiao, and Q. Niu, *Phys. Rev. B* **77**, 235406 (2008).
- [7] H. Zeng, J. Dai, W. Yao, D. Xiao, X. Cui, *Nat. Nanotech.* **7**, 490 (2012).
- [8] K. F. Mak, K. He, J. Shan, and T. F. Heinz, *Nat. Nanotech.* **7**, 494 (2012).
- [9] E. J. Sie, J. W. McIver, Y.-H. Lee, L. Fu, J. Kong, and N. Gedik, *Nat. Mat.* **14**, 290 (2015).
- [10] Y. Ye, J. Xiao, H. Wang, Z. Ye, H. Zhu, M. Zhao, Y. Wang, J. Zhao, X. Yin and X. Zhang, *Nat. Nanotech.* **11**, 598 (2016).
- [11] Z. Wu, F. Zhai, F.M. Peeters, H.Q. Xu, and K. Chang, *Phys. Rev. Lett.* **106**, 176802 (2011).
- [12] C.H. Park, Y.W. Son, L. Yang, M.L. Cohen, S.G. Louie, *Nano Lett.* **8**, 2920 (2008).
- [13] V. V. Cheianov, V. Falco, and B. L. Altshuler, *Science* **315**, 1252 (2007).
- [14] A. G. Moghaddam and M. Zareyan, *Phys. Rev. Lett.* **105**, 146803 (2010).
- [15] F. Goos and H. Hänchen, *Ann. Phys. (Leipzig)* **436**, 333 (1947).
- [16] C.W.J. Beenakker, R.A. Sepkhanov, A.R. Akhmerov, and J. Tworzydło, *Phys. Rev. Lett.* **102**, 146804 (2009).
- [17] F. Zhai, Y. Ma, and K. Chang, *New J. Phys.* **13**, 083029 (2011).
- [18] S. Ghosh, M. Sharma, *J. Phys.: Condens. Matter* **21**, 292204 (2009).
- [19] N. Agrawal, S. Ghosh, and M. Sharma, *Int. J. Mod. Phys. B* **27**, 1341003 (2013).
- [20] Q. Zhang and K.S. Chan, *Appl. Phys. Lett.* **105**, 212408 (2014).
- [21] E.S. Azarova and G.M. Maksimova, *J. Phys. Chem. Sol.* **100**, 143 (2017).
- [22] J.F. Sun and F. Cheng, *J. Appl. Phys.* **115**, 133703 (2014).
- [23] X. Chen, J.-W. Tao, and Y. Ban, *Eur. Phys. J. B* **79**, 203 (2011).
- [24] X. Chen, X.-J. Lu, Y. Ban and C.-F. Li, *J. Opt.* **15** 033001 (2013).
- [25] X. Chen, C.-F. Li, Y. Bana, *Phys. Lett. A* **354** 161 (2006).
- [26] Y. Song, H.-C. Wu, and Y. Guo, *Appl. Phys. Lett.* **100**, 253116 (2012).
- [27] X. Chen, P.-L. Zhao, X.-J. Lu, L.-G. Wang, *Eur. Phys. J. B* **86**,

- 223 (2013).
- [28] A. Saffarzadeh and G. Kirczenow, *Appl. Phys. Lett.* **102**, 173101 (2013).
- [29] X. Li, T. Cao, Q. Niu, J. Shi, and J. Feng, *PNAS* **110**, 3738 (2013).
- [30] Due to a mistake in a minus sign, the authors of Ref. 23 could not obtain Eq. (11) in Ref. 16.
- [31] O. Klein, *Z. Phys.* **53**, 157 (1929).
- [32] C. W. J. Beenakker, *Rev. Mod. Phys.* **80**, 1337 (2008).
- [33] M. I. Katsnelson, K. S. Novoselov, and A. K. Geim, *Nat. Phys.* **2**, 620 (2006).
- [34] The transmission gap is an interval of energy where the critical angle is less than the incident angle, so that the electron wave function in the gated region becomes evanescent. See, X. Chen, J.-W. Tao, *Appl. Phys. Lett.* **94**, 262102 (2009).